Characterization of Heat Loads From Mitigated and Unmitigated VDEs in DIII-D

E.M. Hollmann[1], N. Commaux[2], N.W. Eidietis[3], D.A. Humphreys[3], T.C. Jernigan[2], C.J. Lasnier[4], R.A. Moyer[1], R. Pitts[5], M. Sugihara[5], E.J. Strait[3], J.G. Watkins[6], and J.C. Wesley[3]

[1]*University of California San Diego, 9500 Gilman Dr., La Jolla, CA 92093-0417, USA*
[2]*Oak Ridge National Laboratory, PO Box 2008, Oak Ridge, TN37831, USA*
[3]*General Atomics, PO Box 85608, San Diego, California 9186-5608, USA.*
[4]*Lawrence Livermore National Laboratory, Livermore, CA 94550, USA*
[5]*ITER Organization, St Paul lez Durance 13115, France*
[6]*Sandia National Laboratory, Albuquerque, NM 87185, USA*

The characterization and study of tokamak disruption heat loads is important for predicting wall lifetime in future tokamaks and for designing disruption mitigation systems [1]. Intentional vertical displacement events (VDEs) are an excellent way to study disruption heat loads because they (a) serve as a near worst-case scenario for disruptions heat loads, (b) can be created reliably with repeatable timing, and (c) can be made to move into the lower divertor where good diagnostic coverage exists in DIII-D [2].

The plasmas studied here are lower single null (LSN) shapes heated with 3.5 MW of neutral beam power, giving a total stored energy of $W_{tot} = 1.8$ MJ. At time t = 3 s during the discharge, the plasma shaping coils are used to give the plasma a downward kick. The elongated plasma then goes vertically unstable, drifting into the lower divertor. The x-point disappears around 3025 ms and the plasma then goes into the disruption thermal quench (TQ) around 3030 ms. At the TQ time, the plasma is strongly limited on both the divertor shelf and the inner wall, as shown by magnetic reconstructions (JFIT), Fig. 1.

Currents going into the divertor are monitored with tile current monitors on the divertor shelf – there are seven monitors, toroidally spaced, thus giving some information on the toroidal distribution of halo currents. Electron density and temperature on the lower divertor shelf are measured with a radial array of fixed Langmuir probes. IR emission from the lower divertor is measured with a mid-IR (3–5 μm) camera. To obtain fast time resolution, the IR camera is run in a line scan mode, giving a radial slice of IR brightness across the lower divertor at one

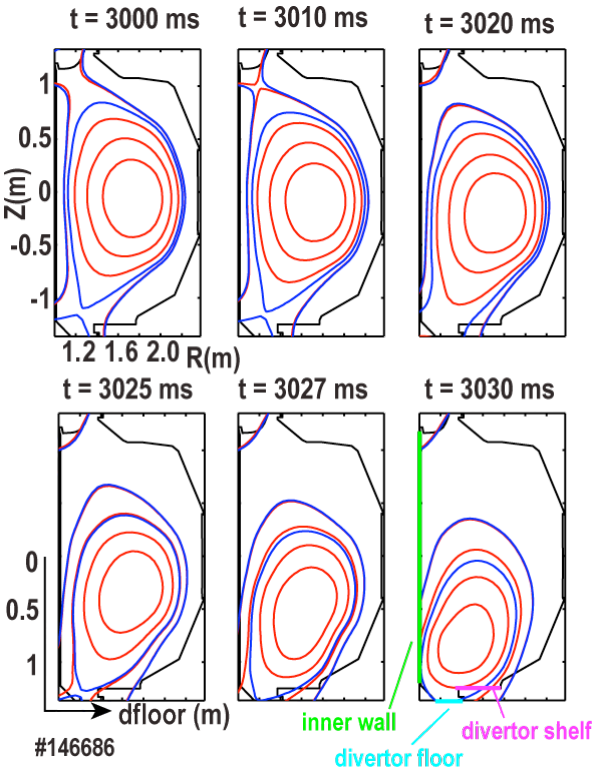

Fig. 1. Magnetic flux surface reconstructions (JFIT) of plasma motion during downward VDE.

toroidal location. C-III (465 nm) emission from the lower divertor is measured with filterscopes (fast PMT/interference filter packages). Total radiated power is measured with AXUV photodiode arrays at two locations – a single fan at toroidal angle $\varphi = 210^{\circ}$ and two crossed fans at $\varphi = 90^{\circ}$. A fast tangentially viewing visible camera is used to view neutral deuterium (D_{α}) emission from the lower main chamber region.

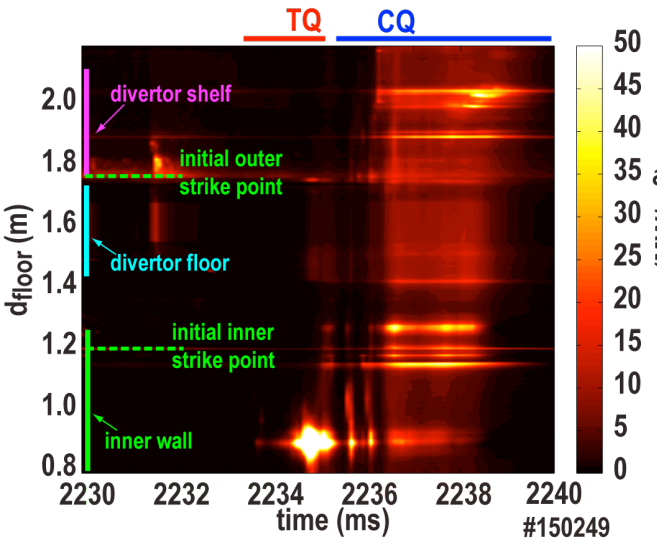

Fig. 2. IR thermography showing heat loads to the inner wall during a VDE.

Figure 2 shows an example of line-scan IR camera heat loads calculated on the lower chamber at one toroidal location. Heat flux as a function of time and d_{floor}, distance across the lower divertor floor, is plotted. It can be seen that the TQ heat loads are not largest at the initial strike points, but on the inner wall. Surprisingly, there is not a corresponding TQ localized heat flux region in the center of the divertor shelf, the other location where the plasma scrape-off layer (SOL) is limiting. Also, the current quench (CQ) heat loads are not smoothly varying with position, as would be expected of radiated heat loads, indicating that some conducted heat loads occur during the CQ.

Evidence for poloidal asymmetries in heat loads are also seen in the structure of visible and UV radiation emitted from the plasma. During VDEs, visible and UV line emission dominantly arises from hydrogen and carbon released from the vessel walls during the TQ and therefore gives some indication of heat loads and plasma flows during the disruption. Figure 3 shows (a) – (d) fast bolometry and (e) – (h) visible (Dα) imaging. Both indicate strong line emission from the lower inner wall and center post, suggesting a strong poloidal asymmetry (inward bias) in the edge heat fluxes and/or plasma flows during the VDE. This conclusion seems to be independent of toroidal magnetic field direction, and the cause of this asymmetry is not known at present.

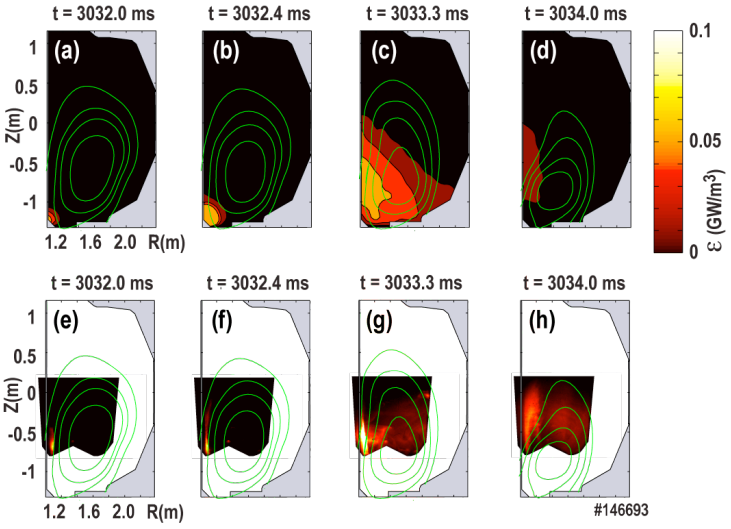

Fig. 3. (a)-(d) fast bolometry showing total plasma emissivity contours and (e)-(f) visible Dα imaging during a VDE.

Understanding the flow of power during disruptions is important for predicting wall damage. Traditionally, the plasma

thermal energy is thought to be lost via heat conduction to the divertor strike points during the TQ, while plasma magnetic energy is thought to be lost via radiation during the CQ. However, exceptions to this have been observed: for example, MAST has seen up to 50% CQ power loss due to conducted heat loads [3] and JET has seen up to 50% CQ power loss due to dissipation in the vessel structure by induced currents [4].

Figure 4 shows estimated power loss from the plasma to the vessel during (a) an unmitigated VDE and (b) a mitigated VDE where massive gas injection was used: 1200 torr-liters of neon was fired into the plasma in a 2 ms long pulse at time Δt_{MGI} = 5 ms after the VDE was triggered. The presence of toroidal asymmetries in heat loads and radiated power complicates analysis of the power flow. Radiated power measurements are available at two toroidal locations, while IR thermography and divertor shelf Langmuir probes are available at one toroidal location. Additionally, the analysis of IR imaging itself is complicated due to the uncertain level of plasma IR emission, plasma radiative heating of the wall, and the uncertain level of loosely bound graphite surface layers. In Fig 4, we plot only IR heat load data from the shelf edge where the localized heat loads are high and plasma radiative contributions can be easily subtracted away. This serves as a qualitative, but not global, indication of conducted heat loads. The induced power loss is estimated from the toroidal vessel current, estimated from internal and external magnetic coils, and from the poloidally-averaged vessel resistivity. It can be seen that the unmitigated VDE has dominantly conducted heat loads initially, followed by significant radiated heat loads at the end of the TQ and during the CQ. As expected, the mitigated VDE has dominantly radiated heat loads during the TQ. Interestingly, conducted heat loads appear to become significant toward the end of the CQ for both mitigated and unmitigated VDEs. Induced power loss appears to be insignificant for both mitigated and unmitigated VDEs.

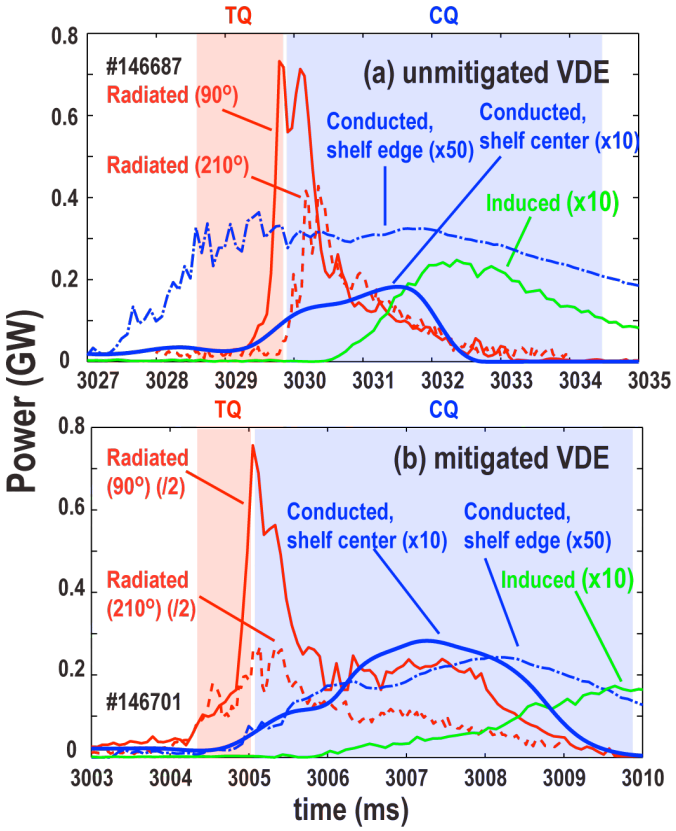

Fig. 4. Comparison of radiated, conducted, and induced power loss during (a) unmitigated and (b) mitigated VDEs. VDEs are triggered at 3000 ms.

To study the effect of the MGI trigger delay Δt_{MGI} on mitigation effectiveness, the delay was varied over the range 5 – 25 ms, with Δt_{MGI} = 30 ms roughly corresponding to the TQ onset time. The resulting trends in effectiveness with Δt_{MGI} are shown in Fig. 5 for various

mitigation metrics. Figure 5(a) shows conducted energy to the shelf center (from Langmuir probes) and to the shelf edge (from IR imaging). Figure 5(b) shows radiated energy from two toroidal locations from fast bolometry assuming toroidal symmetry (i.e. the true total radiated energy is some average between the two traces). Figure 5(c) shows the number of sputtered carbon atoms. This is estimated from fast C-III brightness measurements and is expected to serve as a rough global indicator of conducted heat loads. Figure 5(d) shows the peak toroidal wall currents from tile current monitors. Figure 5(e) shows peak poloidal wall currents from internal and external pickup coils. Figure 5(f) shows the toroidal peaking factor in poloidal wall currents (this times the magnitude of the poloidal wall currents is expected to give a rough indication of vessel forces), and Fig. 5(g) shows the peak vessel vertical displacement (also a rough indicator of vessel forces). Overall, compared with the initial total plasma energy W_{tot} = 1.8 MJ, Fig. 5(b) suggests that the radiated energy fraction is close to 100% for sufficiently early MGI (15 ms or more before the TQ). For later MGI, the radiated power fraction drops about a factor of 2, suggesting that conducted heat loads account for perhaps half of the energy lost. Vessel forces appear to be reduced by perhaps a factor of 2 for sufficiently early MGI.

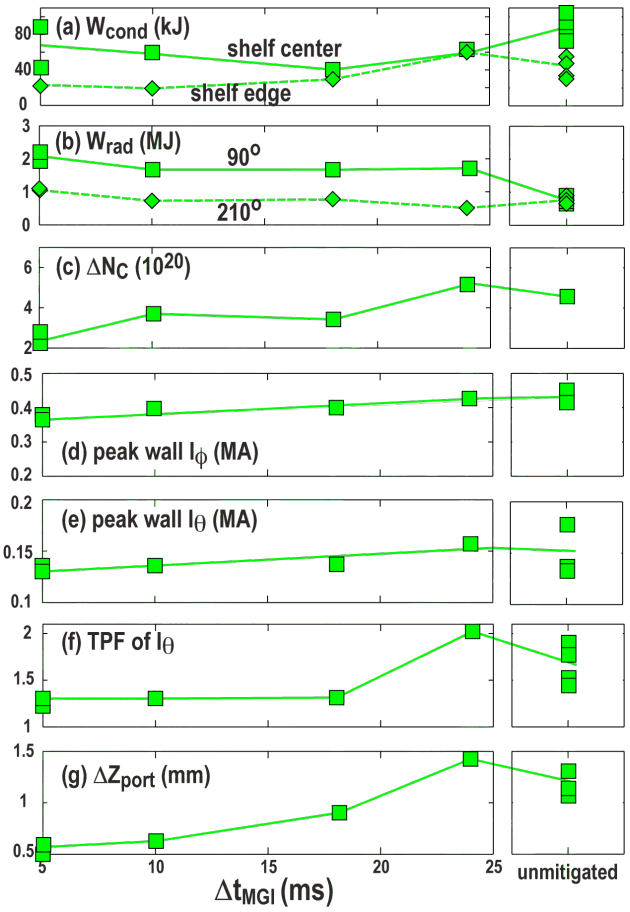

Fig. 5. Effectiveness of neon MGI in mitigating vessel heat loads and forces as a function of trigger delay, showing: (a) conducted energy loss (to some sections of the vessel only), (b) radiated energy loss, (c) sputtered carbon, (d) peak toroidal wall currents, (e) peak poloidal wall currents, (f) toroidal peaking factor of poloidal wall currents, and (g) vertical displacement of vessel.

This work was supported in part by the US Department of Energy under DE-FG02-07ER54917, DE-AC05-00OR22725, DE-FC02-04ER54698, DE-AC52-07NA27344, and DE-AC04-95AL85000.

[1] T.C. Hender, *et al.,* Nucl. Fusion **47**, S128 (2007).

[2] J. L. Luxon, *et al.,* Nucl. Fusion **42** (2002) 614.

[3] A. Thornton, "Heat Flux measurements and disruption mitigation by massive gas injection in JET," (EFDA 2010 meeting of the SEWG transient heat loads, Jülich, 2010).

[4] A. Huber, *et al*., J. Nucl. Mater. **415**, S821 (2011).